

Article

Influence of the Active Phase (Fe, Ni, and Ni–Fe) of Mixed Oxides in CWAO of Crystal Violet

Katherine Archila ¹, Ana María Campos ², Lorena Lugo ², Crispín Astolfo Celis ² ,
Sonia Moreno ¹ , Tomas Ramirez Reina ³  and Alejandro Pérez-Flórez ^{2,*} 

¹ Estado Sólido y Catálisis Ambiental (ESCA), Departamento de Química, Facultad de Ciencias, Universidad Nacional de Colombia, Carrera 30 45-03, Bogotá 110231, Colombia; kgarchilah@unal.edu.co (K.A.); smorenog@unal.edu.co (S.M.)

² Línea de Investigación en Tecnología Ambiental y de Materiales (ITAM), Departamento de Química, Facultad de Ciencias, Pontificia Universidad Javeriana, Carrera 7 No. 43-82, Bogotá 110231, Colombia; amcamposr@yahoo.es (A.M.C.); d.moralesl@javeriana.edu.co (L.L.); crispin.celis@javeriana.edu.co (C.A.C.)

³ Department of Chemical and Process Engineering, University of Surrey, Guildford GU2 7XH, UK; t.ramirezreina@surrey.ac.uk

* Correspondence: alejandroperez@javeriana.edu.co; Tel.: +57-1-3208320 (ext. 4124)

Received: 3 July 2020; Accepted: 27 August 2020; Published: 14 September 2020



Abstract: The catalytic oxidation of aqueous crystal violet (CV) solutions was investigated using Ni and Fe catalysts supported over Mg–Al oxides synthesized by the autocombustion method. The influence of temperature, loading, and selectivity were studied in the catalytic wet air oxidation (CWAO) of CV. The kind of metal had an important contribution in the redox process as significant differences were observed between Fe, Ni, and their mixtures. The catalysts with only Fe as active phase were more efficient for the oxidation of CV under normal conditions ($T = 25\text{ °C}$ and atmospheric pressure) compared to those containing Ni, revealing the influence of the transition metal on catalytic properties. It was found that iron-containing materials displayed enhanced textural properties. The synthesis of Fe/MgAl catalysts by the autocombustion method led to solids with excellent catalytic behavior, 100% CV degradation in eight hours of reaction, 68% selectivity to CO_2 , and significant reduction of chemical oxygen demand (COD).

Keywords: crystal violet; CWAO; autocombustion method; dye; water treatment

1. Introduction

The unsuitable treatment and disposal of industrial wastewater containing dyes has been an environmental problem for decades, limiting the availability of water resources. There are massive concerns about the environmental and health effects of dyes. Synthetic dyes have a detrimental impact even at very low concentrations (1 mg L^{-1}) as they reduce light absorption, thereby having a significant effect on the photosynthetic activity of aquatic plants. They are also related to many diseases, such as cancer, tumors, allergies, heart defects, and others, because of their aromatic structures [1–10]. One of the most common synthetic dyes is crystal violet (CV), which belongs to the family of triarylmethanes and is harmful by inhalation, ingestion, or skin contact. CV dye is also known as a mutagenic agent, carcinogen, and mitotic venom [11–15].

In industries, several technologies have been reported for the elimination of these dyes in wastewater, including adsorption processes, photodegradation, coagulation–flocculation, chemical oxidation, electrochemical oxidation, and biological processes, among others. Several factors, such as high costs, extreme reaction conditions, and the generation of even more polluting waste, disadvantage most of these remediation processes. Because of these issues, research and development of processes that allow the transformation of these residues in an adequate and efficient manner is essential [16–24].

The group of techniques focused on improving the physicochemical characteristics of water bodies is called advanced oxidation processes (AOPs), which are used to eliminate organic compounds in various effluents. In this group, a series of techniques are gathered, such as Fenton, photocatalysis, catalytic oxidation in wet phase (CWAO), and others [25–27].

Unlike other AOPs, CWAO is appropriate for a high organic load and high flow rate. It can also partially cover the range of applications of other methods, such as incineration and biological techniques [28–30]. Additionally, CWAO is capable of mineralizing all organic compounds and inorganic compounds such as cyanide and ammonia using air or oxygen as an oxidizing agent [31]. The appropriate catalyst design can make it possible to have reactions in moderate temperature and pressure conditions compared to other techniques, thereby reducing the cost of the process. However, most of the studies that have used the CWAO technique have operated under considerably high pressure and temperature conditions ($T \approx 120\text{--}150\text{ }^{\circ}\text{C}$ and $P \approx 25\text{--}60\text{ bar}$) [1,30–33].

Numerous types of catalysts have been studied for CWAO of wastewater, which include noble metals, metal oxides, and mixed oxides, and it has been found that the total surface of the solid and good dispersion of the active phase have a significant effect on the speed of reaction. Among the heterogeneous catalysts used for this particular reaction are those based on noble metal systems, such as Pd, Pt, and Au, which are very effective, and certain transition oxides, such as Fe, Ni, Co, Mn, and Cu, which may be less active. However, they have the advantage of being more economical and resistant to poisoning [34].

Along with catalyst design, synthesis plays a fundamental role as the textural, structural, and catalytic properties of solids are modulated. In the search for methods that allow better control of particle size, metallic dispersion, and greater surface area, autocombustion appears as an interesting, versatile, and accessible method for the preparation of mixed oxides. During the autocombustion process, the evolution of gaseous products leads to dissipation of heat, thereby limiting the increase in temperature and reducing sintering. In turn, this method leads to porous structures, which facilitate the adsorption and diffusion of the reactant molecules, and generates materials with high surface area, narrow particle size range, better distribution of particles, and high phase purity.

Regarding the metal used for these catalysts, nickel and iron have been shown to be the most efficient in carrying out oxidation reactions [1,35,36]. For this reason, they were selected in this work as constitutive elements of the active phase for CV removal. On the other hand, a Mg and Al matrix was used as Mg is expected to offer the basic reaction medium while aluminum generates a type of attachment with the CV aromatic groups.

The present work deals with the synthesis, characterization, and testing of the CWAO of CV, with Ni and Fe catalysts supported over Mg–Al mixed oxides synthesized by the autocombustion method. The catalysts that were developed operated under moderate environmental conditions of reaction, and 100% degradation of CV was reached at just 8 h of reaction. The results are much better than those currently reported in the literature [25].

2. Results

2.1. Characterization

Thermogravimetric analysis (TGA) of NiFe (0:1) mixed oxides is presented in Figure 1. It can be seen that oxides calcined at temperatures below $700\text{ }^{\circ}\text{C}$ showed losses above 35%, indicating that nitrate and glycine residues were still present. For the solid calcined at $700\text{ }^{\circ}\text{C}$, the loss was only 17%, which basically corresponds to water [34].

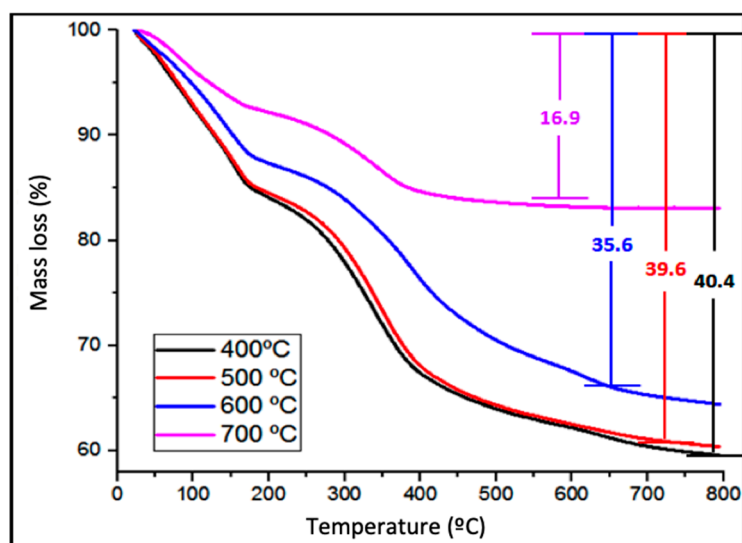


Figure 1. Thermogravimetric analysis (TGA) of NiFe (0:1) mixed oxides calcined at different temperatures.

Regarding the structural analysis of the mixed oxides, the XRD patterns (Figure 2) indicated that the catalyst with Ni had NiO as the predominant phase, with the main peak at $43.1^\circ 2\theta$ and a secondary peak located at $62.6^\circ 2\theta$ (JCPDS No 89–7130). Other characteristic planes of this phase are at 33.3° and 75.5° [32]. Solids containing Fe showed the phase corresponding to magnetite ($\text{Fe}^{2+} \text{Fe}_2\text{O}_4$) at angles 2θ of 30° , 35.5° , 42.7° , 56.1° , and 61.5° (FeO , JCPDS No 85-0625; Fe_3O_4 JCPDS No 75-1609) [36].

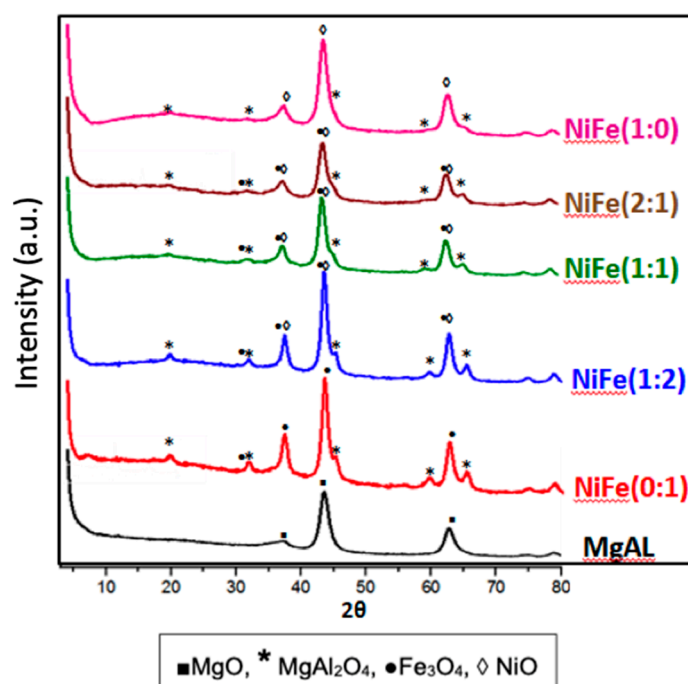


Figure 2. XRD profiles of mixed Ni–Fe oxides.

Furthermore, in all solids, the spinel phase (MgAl_2O_4) with the characteristic plane at $2\theta = 36.7^\circ$ was present (JCPDS No. 21–11052). These results are conclusive regarding the successful synthesis of mixed oxides by the self-combustion method, generating active phases that are responsible for the oxidation processes [1,35]. The catalysts containing both Ni and Fe metals had a combination of the two phases without shifting the characteristic planes. Finally, the support MgAl, which does not

contain an active phase but is essential in order to promote basic properties of the material, exhibited the periclase phase (MgO) and did not reveal segregated aluminum phases.

Additionally, by means of this technique, it was possible to determine the size of the crystallites of the solids with good approximation. Here, it is necessary to use the Scherrer equation, where K is the form factor with a value of 1, λ is the wavelength that is influenced in the analysis corresponding to the λ of Cu (nm), θ is the Bragg angle, β is the mean height width (FMWH), and τ is the average grain size. For mixed oxides with Fe, the FMWH of the plane in $2\theta = 35.5^\circ$ was characteristic of Fe_3O_4 and for those with Ni, the $2\theta = 43.1^\circ$ corresponded to NiO [35,36].

As summarized in Table 1, the crystallite sizes of the synthesized solids were between 2 and 4 nm. The nature of the active phase did not seem to influence the size of the crystallite as these were similar for both Ni or Fe as the active metal.

Table 1. Textural properties of synthesized solids and size of crystal oxide of the active phase.

Catalyst	S_{BET}	Pore Volume ($\text{cm}^3 \text{g}^{-1}$)	FMWH_{Fe}	τ_{Fe} (nm)	FMWH_{Ni}	τ_{Ni} (nm)
MgAl	211	0.286	-	-	-	-
NiFe (0:1)	85	0.180	0.703	3	-	-
NiFe (1:2)	80	0.171	0.624	4	0.699	2
NiFe (1:1)	70	0.135	0.779	3	0.739	2
NiFe (2:1)	75	0.120	0.748	3	0.532	3
NiFe (1:0)	75	0.136	-	-	0.592	2

The adsorption isotherms of the mixed NiFe/MgAl oxides are shown in Figure 3. All the oxides showed type IV isotherms (IUPAC classification) corresponding to mainly mesoporous materials with H3 type hysteresis loops [37,38]. It is evident that the nature of metal of the active phase did not have an important effect on the area of the synthesized solids as all the oxides had areas close to $80 \text{ m}^2 \text{ g}^{-1}$ and a pore volume of $0.120\text{--}0.180 \text{ cm}^3 \text{ g}^{-1}$ (Table 1). However, the MgAl support was characterized by a high specific surface area and a large pore volume ($0.286 \text{ cm}^3 \text{ g}^{-1}$). It was reduced with the introduction of Ni and Fe metals. This was probably due to the blockage in the MgAl phase, which reduced the surface area of the final material due to the presence of very small NiO and Fe_2O_3 particles (2–4 nm) (Table 1).

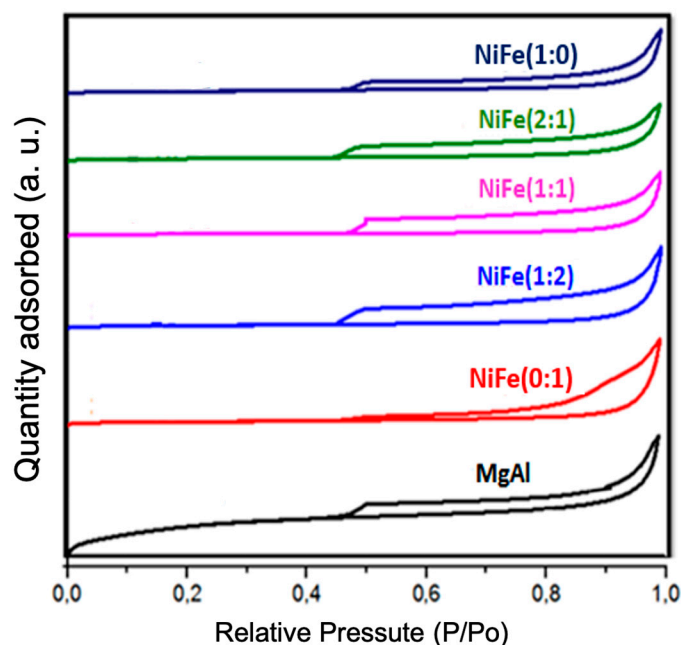


Figure 3. Nitrogen adsorption/desorption isotherms for mixed oxides.

Figure 4 shows the H₂-TPR profiles of mixed oxides, with the reducibility of iron, nickel, and the mixture of both analyzed. The samples containing Fe had a fairly wide profile associated with multiple oxidation states and different chemical environments of iron. Two zones of reducibility for iron were clearly observed from 220 to 700 °C, which corresponded to the oxidation states of Fe³⁺ to Fe²⁺, Fe²⁺ to Fe⁺, and Fe⁺ to Fe⁰. At temperatures above 700 °C, the species strongly linked to the MgAl support [36,39].

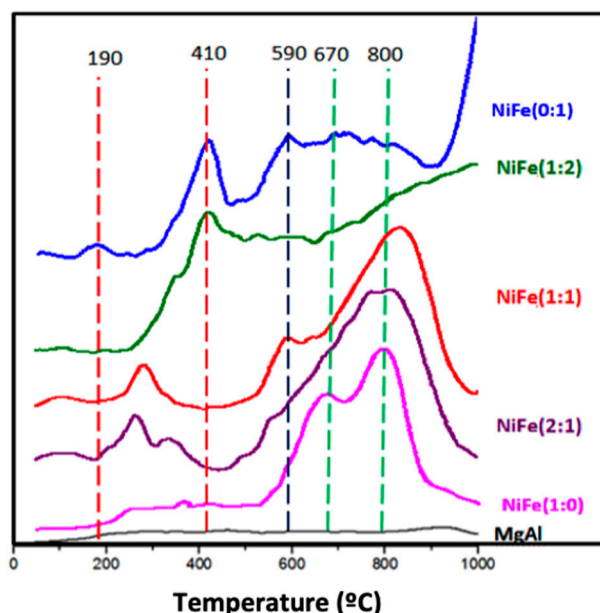


Figure 4. H₂-TPR profiles of NiFe/MgAl mixed oxides.

The TPR-H₂ profile of the solid with only nickel as active metal (NiFe (1:0)) indicated that the presence of Mg²⁺ and Al³⁺ ions induced a decrease in the reducibility of Ni²⁺ [40,41]. A peak of maximum reduction between 700 and 900 °C was obtained, corresponding to the reduction of NiO, which is in strong interaction with the matrix of Mg and Al oxides [40,42]. Likewise, reductions appeared at lower temperatures (550–672 °C), which are associated with free NiO.

Related to mixed Ni–Fe oxides, a shift to lower reduction temperatures was observed compared with NiFe (1:0) solid. These profiles are very complex to interpret due to the high number of possible combinations of different oxidation states for both iron and nickel that may be present, as indicated in the XRD analysis. However, it could be established that the region between 300 and 700 °C corresponded to the reduction of Fe³⁺ to Fe²⁺ species, from Fe²⁺ to Fe⁺, and of Ni²⁺ to Ni⁺ species, while the peaks centered around 820 °C corresponded mainly to the transition from nickel Ni⁺ to Ni⁰ species [40,42]. The displacement of the profiles at lower temperatures was because of the inclusion of iron, which gave better dispersion of the Ni phases present in the catalyst [42]. In general, it can be concluded that iron facilitates the reduction of metallic nickel at lower temperature values, possibly obtaining more active solids in oxidation reactions under moderate conditions.

On the other hand, and based on the consumption of H₂, it was possible to determine that NiFe (0:1) had the highest reducibility percentage (95%) compared to the other mixed oxides (Table 2). This probably influenced the catalytic activity.

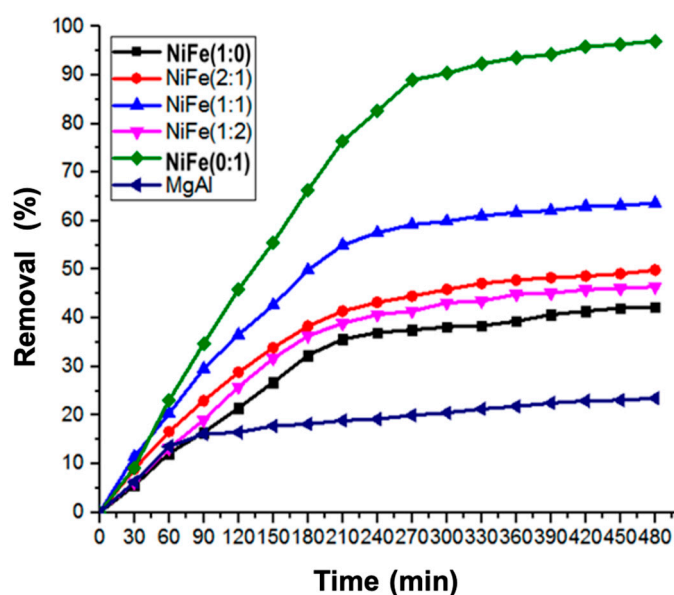
Table 2. TPR-H₂ for NiFe/MgAl mixed oxides. Ratios determined by X-ray fluorescence (XRF).

Solid	Temperature of High Reduction (°C)	Reducibility (%)	Ni/Al	Ratios Fe/Al	Mg/Al
NiFe (0:1)	190 y 410	95	-	0.4	1.8
NiFe (1:2)	410	46	0.1	0.3	1.8
NiFe (1:1)	270, 590 y 850	78	0.2	0.2	1.7
NiFe (2:1)	250 y 850	48	0.3	0.1	1.8
NiFe (1:0)	670 y 820	46	0.4	-	1.8

Regarding the chemical composition by X-ray fluorescence (XRF) (Table 2) indicated through molar relationships between the elements, the catalysts revealed a similar and consistent chemical composition with the nominal ratio used in the synthesis, highlighting that the autocombustion method allows solids to be obtained without loss of the nominal value.

2.2. Catalytic Activity

The catalytic activity at 25 °C was evaluated in the wet air oxidation of CV as mentioned above and chosen as a representative model molecule of recalcitrant dyes. Figure 5 shows the catalytic behavior of mixed oxides (NiFe/MgAl). It can be seen that the solid with only Fe as the active phase showed the best results (100% of elimination in 8 h of reaction).

**Figure 5.** Catalytic conversion of crystal violet (CV) at 25 °C with NiFe/MgAl oxides.

The excellent results obtained with iron as the active phase compared to the catalyst that only contained nickel as the active phase might be associated with the various oxidation states of the metal that assist the oxide-reducing processes. Additionally, a cooperative effect between Fe and Ni could be verified with respect to the activity of the solid with only Ni as the active phase.

As the highest catalytic activity was observed with NiFe (0:1) solid (only Fe as the active phase), subsequent experiments were carried out only with this catalyst.

3. Discussion

In general, it has been reported that high temperatures are needed in order to successfully degrade dyes [1,16]. This research considered the use of moderate conditions by lowering the commonly used temperature of 70 °C [1,32] to normal conditions (25 °C and atmospheric pressure).

The results of shifting the temperature from 70 to 19 °C are detailed in Figure 6, where it is clear that the removal rate is directly related to the temperature used. With a temperature of 70 °C,

total oxidation of CV was achieved in just 30 min. As the temperature decreased, the transformation speed became slower until reaching a temperature of 19 °C, where the speed and oxidation of CV decreased. Finally, for the evaluation of the other parameters of interest, the temperature of 25 °C was chosen. It was found that total oxidation of the CV occurred in 8 h of reaction, a result that even exceeds some reports in the literature [25], achieving removal of the CV with a Ni–MgAl catalyst under extreme reaction conditions ($T = 120\text{--}180\text{ }^{\circ}\text{C}$, $P = 60\text{ bar}$, and air flow 300 mL min^{-1}) with 44.7–86.1% of CV elimination in 12 h of reaction.

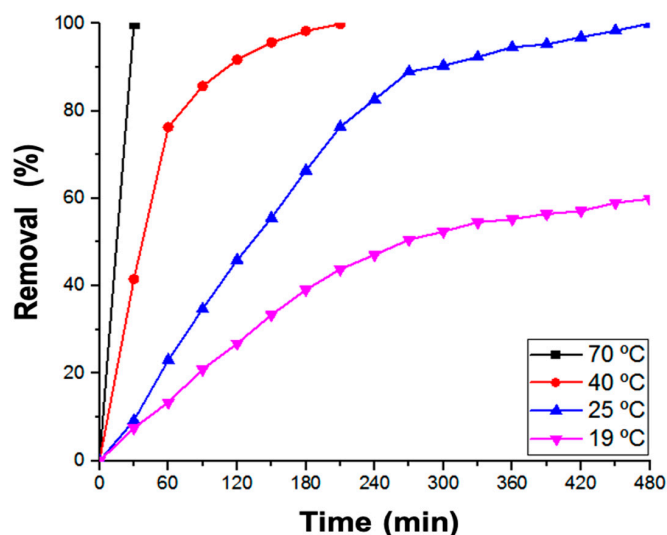


Figure 6. Effect of temperature on CV conversion with NiFe (0:1) catalyst at normal pressure.

Figure 7 illustrates some results of blank tests that allowed evaluation of the effect of the presence of catalyst on the reaction medium. It is evident that the degradation of the dye during the reaction period was quite rapid in the presence of the catalyst and oxygen in the reaction medium (CWAO process), while the degradation occurred in a much less effective way (did not exceed 10%) without the presence of the catalyst in the solution (without catalyst, with air/without catalyst). Clearly, the presence of the catalyst allowed the formation of $\text{OH}\bullet$ radicals that carried out the CWAO reaction, as indicated in the chain reaction in Figure 8.

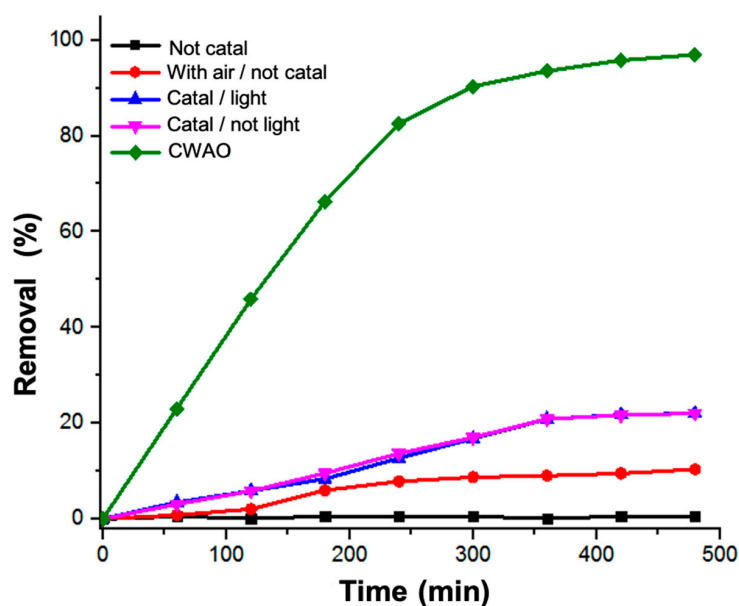


Figure 7. Evaluation of the effect of catalyst on the reaction (NiFe (0:1)).

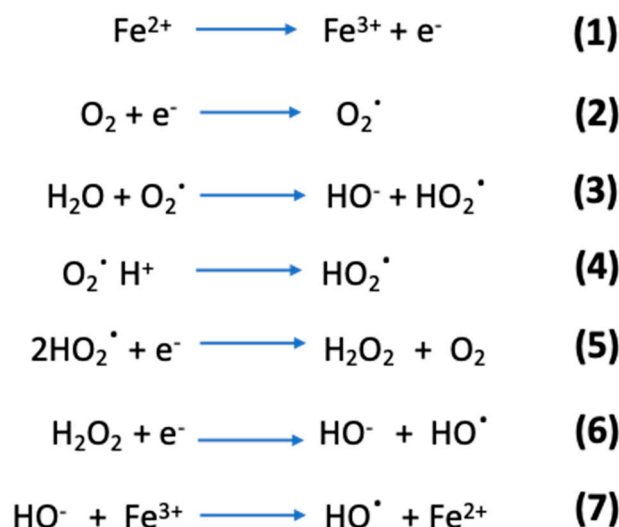


Figure 8. Chain reactions for catalytic wet air oxidation (CWAO) process [43].

The vast majority of dyes are photosensitive, which means they are unstable in the presence of light, thereby enabling their degradation in its presence. In Figure 7, it can be observed that regardless of the presence or absence of light (catal/light or catal/no light respectively), the CV was very stable and was not affected, with identical results for the two tests. This demonstrates that it is not a photocatalytic process and that the degradation was mainly governed by a CWAO process.

Selectivity in CV Reaction

One of the parameters for assessment is selectivity and the reduction of chemical oxygen demand (COD). Wastewater generated by some industries includes organic compounds that are toxic, with a high level of total organic carbon (TOC) and low biodegradability [43]. It is necessary to verify these kinds of compounds in the catalytic reaction in order to discard the effluents as required by environmental legislation.

Table 3 summarizes the results of CV elimination and CO₂ selectivity, both measured as TOC and COD reduction percentage after 8 h of reaction. Catalyst NiFe (0:1) was not only the most active but also the most selective, reaching 68% of TOC and a decrease in COD of 60%.

Table 3. Chemical oxygen demand (COD) and reaction parameters in the CWAO of CV.

Catalyst	Elimination (%)	TOC (%)	DQO (%)
MgAl	20	9	0
NiFe (0:1)	100	68	60
NiFe (1:2)	44	29	13
NiFe (1:1)	60	61	28
NiFe (2:1)	50	30	26
NiFe (1:0)	42	29	13

In order to accurately monitor the selectivity of the reaction and follow the formation of by-products during CV oxidation, an Agilent 5975 mass-coupled gas chromatograph (CG-MS) was used. Analysis of the products allowed us to conclude that the catalysts have a unique reaction pathway “hydroxyl radical production”, which are produced when the active phase is oxidized by the oxygen included as an external source (air). In this way, superoxide radicals are produced, and hydroxyl radicals are subsequently generated with water; this is the starting point of the CWAO process [44,45]. On the other hand, the other metals in the catalyst (Mg and Al) have a specific function. Aluminum fixes the molecule by the aromatic rings on the catalyst, and magnesium is related to the basic properties of the catalyst and the solution as acidic pH is not suitable in this type of process [45]

Table 4 shows the intermediate compounds in CV oxidation. It was analyzed by the ions and molecular fragments found using GC-MS data compiled in the NIST library. The results demonstrated that selectivity depended on the active phase of the catalyst as the solids with Ni generated residues with longer carbon chains and double bounds. In contrast, the NiFe solid (0:1) was more selective in generating saturated alcohols and amines. Therefore, it can be concluded that this catalyst is the best for CV degradation processes.

Table 4. Compounds produced during CV oxidation analyzed by GC-MS.

Time (h)	NiFe (0:1)	NiFe (1:1)	NiFe (1:2)—NiFe (2:1)—NiFe (1:0)
0		CV	
2		Ethylbenzene, p, m and o-xylene	
4	Propylamine 1,2-diethoxyethane Aminoacetidrazide	Isobutylcyclopentane Dipropylene glycol Toluene	1,1-diethoxyethane 1,3-dioxolane 2-hydroxypropyl ether butylamine
6	2-hexanol 3-nitropropionic acid 1,1-diethoxyethane Carbon dioxide	1-Chloro-2,3-epoxypropane Acetylmethylamine	3-hexenylbutyrate dibutyl oxalate 1,3-dimethyl urea 2-heptenal
8	4-amino-1-butanol 2-Methyl-2-butanol Propylamine	Oxirane 1-Methoxy-2-methyl -2-propanol	2-isobutyl-2-propenol aminoacetonitrile propionamide n-methylacetidine 3-aminopropene

4. Materials and Methods

4.1. Catalyst Synthesis

The mixed oxides were synthesized from hydrated nitrate solutions by the autocombustion method. For the synthesis of FeMgAl, NiMgAl, and NiFeMgAl catalysts, Mg^{2+} , Al^{3+} , Fe^{2+} , and Ni^{2+} nitrates (Merck, over 95% purity) were used as oxidants reagents, and glycine (CH_2NH_2COOH) (Merck analytical degree) was used as combustible. Molar ratios for the preparation M^{2+}/Al^{3+} were 3 ($M^{2+} = Mg + Ni$ or Fe) and $NO_3^-/glycine = 0.8$. These solids are named with the atomic symbol of the active phase and have a number in parentheses that corresponds to the concentration of the active phase in mmol.

The synthesis involved four stages. The first stage was based on the mixture of nitrates with glycine in an aqueous solution with constant stirring. In the second step, the obtained solution was evaporated at 90–100 °C, keeping the stirring constant until a gel was formed. Subsequently, the gel was heated to 500 °C so that the ignition that would form the respective oxide and the gaseous products occurred. Finally, the system was cooled down. The oxides obtained were calcined at 700 °C for 14 h to remove the residues of glycine and nitrates that were still present [34]. The choice of the calcination temperature was based on the study of the said parameter on the stability of the final solid, for which temperatures of 400, 500, 600, and 700 °C were evaluated. The oxides evaluated for CV degradation revealed the greatest degradation with the oxide at 700 °C.

4.2. Characterization

TGA was carried out under airflow conditions of 60 mL min^{-1} and with a heating rate of 10 °C min^{-1} up to 800 °C using TA DSC-TGA SDT Q 600. XRD (powder sample) using a Panalytical X'pert PRO MPD diffractometer equipped with a copper anode ($\lambda = 1.5406$ Å) and with an angular

velocity of $1^\circ/\text{min}$ and step size of $0.02^\circ \theta$ was carried out to evaluate the crystalline phases. The chemical analysis of catalysts was carried out using the XRF technique on a Philips MagiX Pro PW2440 device (tube with Rh with 4 Kw). The samples were prepared in the form of pearls (melted glass) for which the following was used as a flux mixture: lithium tetraborate/lithium metaborate in a ratio of 60:40 and as nonstick LiI, and 0.8 g of sample, for a total weight of 8 g pearl. The textural characteristics were determined through N_2 adsorption–desorption isotherms using ASAP 2020 Micrometitics equipment.

The oxidative–reductive properties of the materials were measured by means of TPR- H_2 in a CHEMBET 3000 QUANTACHROME equipment, where the reduction was carried out with a gaseous mixture of H_2/Ar 10% *v/v* (30 mL min^{-1}) and a heating ramp of $10^\circ\text{C}/\text{min}$.

4.3. Catalytic Evaluation

A Thermo Scientific GENESYS 20 spectrophotometer was used to measure the CV concentration. Analyses were carried out in a quartz cell, and the dye concentration was measured at the fixed wavelength (590 nm) corresponding to the maximum absorbance for CV. The selectivity evaluation was performed with a TOC-L CPH analyzer, which uses a nondispersive infrared detector to quantitatively analyze the carbon dioxide originating from the sample.

The COD measurement was performed using kits reference HI93754A-25 COD LR for the analysis of the samples in this work. The preparation of the samples for the analysis in CG-MS Agilent 5975 was done by the extraction of the sample with dichloromethane to separate the aqueous phase, where a 1:10 ratio (sample: solvent) was used. A DB5 column $60 \text{ m} \times 0.25 \text{ mm}$ was used. The column temperature was programmed with three heating ramps. The first temperature at 40°C was maintained for 4 min. It was then raised to 80°C with a speed of 4°C min^{-1} and held for 2 min. Finally, it was raised to 320°C at 8°C min^{-1} and held for 9 min. Helium was used as a stripping gas with a flow of 5.79 mL min^{-1} ; the injector temperature was 220°C , with a sample injection volume of $1 \mu\text{L}$. The mass/charge ratio evaluated for this method was between 10 and 300 m/z .

5. Conclusions

The synthesis of NiFe/MgAl solids by the autocombustion method led to solids with excellent catalytic behavior, 100% CV degradation in eight hours of reaction, 68% selectivity to CO_2 , and significant reduction of COD.

The type of metal in the main active phase had a significant impact on the redox process, and indeed remarkable differences were observed between Fe, Ni, and their mixtures. The catalysts with only Fe as active phase was more efficient for CV oxidation under normal conditions of temperature and pressure ($T = 25^\circ\text{C}$ and atmospheric pressure) compared to those containing Ni, revealing the significance of the physicochemical properties of the transition metal.

Regarding the iron content, it was found that solids with a lower load of Fe had an improvement in their textural properties. In addition, when nominal load of iron was 5 mmol (NiFe (0:1)), both textural and redox properties were the most appropriate, achieving around 100% removal of CV dye in eight hours.

The reaction mechanism for all solids was the same, tuning the activity and selectivity of the process, which was defined by the reaction rate on each catalyst. Thus, in solids with Ni as the active phase, the reaction was slower, which might favor rearrangements of the molecules and lower selectivity to CO_2 and H_2O . Overall, this work showcases a successful strategy to design economically viable catalysts for water purification via oxidation catalysis.

Author Contributions: Formal analysis, A.P.-F.; investigation, S.M.; methodology, K.A. and L.L.; project administration, C.A.C.; resources, T.R.R.; supervision, A.P.-F.; writing—review and editing, A.M.C. All authors have read and agreed to the published version of the manuscript.

Funding: This research was funded by Pontificia Universidad Javeriana, Bogotá, Colombia, Proyecto ID 00007181.

Acknowledgments: Thanks to the Pontificia Universidad Javeriana for the mobility project “Preparation and evaluation of mixed Ce-Ni/Fe oxides by auto-combustion for wet catalytic oxidation of dyes”, ID 20064, which allowed mobility to the University of Surrey to carry out some characterization tests.

Conflicts of Interest: The authors declare no conflict of interest.

References

1. Vallet, A.; Ovejero, G.; Rodríguez, A.; Peres, J.A.; García, J. Ni/MgAlO regeneration for catalytic wet air oxidation of an azo-dye in a trickle-bed reactor. *J. Hazard. Mater.* **2013**, *244–245*, 46–53. [[CrossRef](#)] [[PubMed](#)]
2. Sahoo, C.; Gupta, A.K.; Pal, A. Photocatalytic degradation of Crystal Violet (C.I. Basic Violet 3) on silver ion doped TiO₂. *Dye. Pigment.* **2005**, *66*, 189–196. [[CrossRef](#)]
3. Xu, Y.; Chen, X.; Li, Y.; Ge, F.; Zhu, R. Quantitative structure–property relationship (QSPR) study for the degradation of dye wastewater by Mo–Zn–Al–O catalyst. *J. Mol. Liq.* **2016**, *215*, 461–466. [[CrossRef](#)]
4. Elkady, M.F.; Ibrahim, A.M.; Abd El-Latif, M.M. Assessment of the adsorption kinetics, equilibrium and thermodynamic for the potential removal of reactive red dye using eggshell biocomposite beads. *Desalination* **2011**, *278*, 412–423. [[CrossRef](#)]
5. Zhang, W.; Li, H.J.; Kan, X.W.; Dong, L.; Yan, H.; Jiang, Z.W.; Yang, H. Adsorption of anionic dyes from aqueous solutions using chemically modified straw. *Bioresour. Technol.* **2012**, *117*, 40–47. [[CrossRef](#)]
6. Zhang, Y.; Zhang, Z.; Yan, Q.; Wang, Q. Synthesis, characterization, and catalytic activity of alkali metal molybdate/ α -MoO₃ hybrids as highly efficient catalytic wet air oxidation catalysts. *Appl. Catal. A Gen.* **2016**, *511*, 47–58. [[CrossRef](#)]
7. Chaibakhsh, N.; Ahmadi, N.; Zanjanchi, M.A. Use of *Plantago major* L. as a natural coagulant for optimized decolorization of dye-containing wastewater. *Ind. Crops Prod.* **2014**, *61*, 169–175. [[CrossRef](#)]
8. Liang, C.Z.; Sun, S.P.; Li, F.Y.; Ong, Y.K.; Chung, T.S. Treatment of highly concentrated wastewater containing multiple synthetic dyes by a combined process of coagulation/flocculation and nanofiltration. *J. Membr. Sci.* **2014**, *469*, 306–315. [[CrossRef](#)]
9. Yuan, M.J.; Wang, S.T.; Wang, X.H.; Zhao, L.L.; Hao, T.H. Removal of organic dye by air and macroporous ZnO/MoO₃/SiO₂ hybrid under room conditions. *Appl. Surf. Sci.* **2011**, *257*, 7913–7919. [[CrossRef](#)]
10. Vakili, M.; Rafatullah, M.; Salamatinia, B.; Abdullah, A.Z.; Ibrahim, M.H.; Tan, K.B.; Gholami, Z.; Amouzgar, P. Application of chitosan and its derivatives as adsorbents for dye removal from water and wastewater: A review. *Carbohydr. Polym.* **2014**, *113*, 115–130. [[CrossRef](#)]
11. Au, W.; Parhak, S.; Collie, C.J.; Hsu, T.C. Cytogenetic Toxicity of Gentian Violet and Crystal Violet on Mammalian Cells In Vitro. *Mutat. Res.* **1978**, *58*, 269–276. [[CrossRef](#)]
12. Rai, P.; Gautam, R.K.; Banerjee, S.; Rawat, V.; Chattopadhyaya, M.C. Synthesis and characterization of a novel SnFe₂O₄@activated carbon magnetic nanocomposite and its effectiveness in the removal of crystal violet from aqueous solution. *J. Environ. Chem. Eng.* **2015**, *3*, 2281–2291. [[CrossRef](#)]
13. Nezamzadeh-Ejehieh, A.; Banan, Z. Sunlight assisted photodecolorization of crystal violet catalyzed by CdS nanoparticles embedded on zeolite A. *Desalination* **2012**, *284*, 157–166. [[CrossRef](#)]
14. Lellis, B.; Fávoro-Polonio, C.Z.; Pamphile, J.A.; Polonio, J.C. Effects of textile dyes on health and the environment and bioremediation potential of living organisms. *Biotechnol. Res. Innov.* **2019**, *3*, 275–290. [[CrossRef](#)]
15. Gupta, A.K.; Pal, A.; Sahoo, C. Photocatalytic degradation of a mixture of crystal violet (basic violet 3) and methyl red dye in aqueous suspensions using Ag⁺ doped TiO₂. *Dyes Pigment.* **2006**, *69*, 224–232. [[CrossRef](#)]
16. Yin, J.; Cai, J.; Yin, C.; Gao, L.; Zhou, J. Degradation performance of crystal violet over CuO@AC and CeO₂-CuO@AC catalysts using microwave catalytic oxidation degradation method. *J. Environ. Chem. Eng.* **2016**, *4*, 958–964. [[CrossRef](#)]
17. Chen, Q.; Yu, P.; Huang, W.; Yu, S.; Liu, M.; Gao, C. High-flux composite hollow fiber nanofiltration membranes fabricated through layer-by-layer deposition of oppositely charged crosslinked polyelectrolytes for dye removal. *J. Membr. Sci.* **2015**, *492*, 312–321. [[CrossRef](#)]
18. Reddy, K.R.; Hassan, M.; Gomes, V.G. Hybrid nanostructures based on titanium dioxide for enhanced photocatalysis. *Appl. Catal. A Gen.* **2015**, *489*, 1–16. [[CrossRef](#)]

19. Reddy, K.R.; Nakata, K.; Ochiai, T.; Murakami, T.; Taketoshi, D.A.; Fujishima, A. Nanofibrous TiO₂-core/conjugated polymer-sheath composites: Synthesis, structural properties and photocatalytic activity. *J. Nanosci. Nanotechnol.* **2010**, *10*, 7951–7957. [[CrossRef](#)]
20. Vijayalakshmi, S.R.; Muthukumar, K. Improved biodegradation of textile dye effluent by coculture. *Ecotox. Env. Saf.* **2015**, *114*, 23–30. [[CrossRef](#)]
21. Kebria, M.R.S.; Jahanshahi, M.; Rahimpour, A. SiO₂ modified polyethyleneimine—Based nanofiltration membranes for dye removal from aqueous and organic solutions. *Desalination* **2015**, *367*, 255–264. [[CrossRef](#)]
22. Rondon, H.; El-Cheikh, W.; Boluarte, I.A.R.; Chang, C.Y.; Bagshaw, S.; Farago, L. Application of enhanced membrane bioreactor (eMBR) to treat dye wastewater. *Bioresour. Technol.* **2015**, *183*, 78–85. [[CrossRef](#)] [[PubMed](#)]
23. Punzi, M.; Anbalagan, A.; Börner, R.A.; Svensson, B.M.; Jonstrup, M.; Mattiasson, B. Degradation of a textile azo dye using biological treatment followed by photo—Fenton oxidation: Evaluation of toxicity and microbial community structure. *Chem. Eng. J.* **2015**, *270*, 290–299. [[CrossRef](#)]
24. Vaiano, V.; Sacco, O.; Sannino, D.; Ciambelli, P. Nanostructured N-doped TiO₂ coated on glass spheres for the photocatalytic removal of organic dyes under UV or visible light irradiation. *Appl. Catal. B Environ.* **2015**, *170–171*, 153–161. [[CrossRef](#)]
25. Fernández, C.; Larrechi, M.S.; Callao, M.P. An analytical overview of processes for removing organic dyes from wastewater effluents. *TrAC Trends. Anal. Chem.* **2010**, *29*, 1202–1211. [[CrossRef](#)]
26. Jones, K.; Maxwell, F.R.; Morgan, S.N.; Thornthwaite, D.W. Process for Bleaching Naturally Occurring Oils and Fats. U.S. Patent No. 4,325,883, 20 April 1982.
27. Pizarro, A.H. Decoloration of organic dyes in aqueous phase by catalytic hydrotreatment. *Catal. Commun.* **2017**, *90*, 100–105. [[CrossRef](#)]
28. Kim, K.H.; Ihm, S.K. Heterogeneous catalytic wet air oxidation of refractory organic pollutants in industrial wastewaters: A review. *J. Haz. Mat.* **2011**, *186*, 16–34. [[CrossRef](#)]
29. Hancock, F.E. Catalytic strategies for industrial water re-use. *Catal. Today* **1999**, *53*, 3–9. [[CrossRef](#)]
30. Mishra, V.S.; Mahajani, V.V.; Joshi, J.B. Wet air oxidation. *Ind. Eng. Chem. Res.* **1995**, *34*, 2–48. [[CrossRef](#)]
31. Bhargava, S.K. Wet Oxidation and Catalytic Wet Oxidation. *Ind. Eng. Chem. Res.* **2006**, *45*, 1221–1258. [[CrossRef](#)]
32. Ovejero, G.; Rodríguez, A.; Vallet, A.; García, J. Ni/Fe-supported over hydrotalcites precursors as catalysts for clean and selective oxidation of Basic Yellow 11: Reaction intermediates determination. *Chemosphere* **2013**, *90*, 1379–1386. [[CrossRef](#)] [[PubMed](#)]
33. Dil, E.A.; Ghaedi, M.; Ghaedi, A. Application of artificial neural network and response surface methodology for the removal of crystal violet by zinc oxide nanorods loaded on activated carbon: Kinetics and equilibrium study. *J. Taiwan Inst. Chem. Eng.* **2016**, *59*, 210–220. [[CrossRef](#)]
34. Castaño, M.H.; Molina, R.; Moreno, S. Mn–Co–Al–Mg mixed oxides by auto-combustion method and their use as catalysts in the total oxidation of toluene. *J. Mol. Catal. A Chem.* **2013**, *370*, 167–174. [[CrossRef](#)]
35. Campos, A.; Riaño, P.; Lugo, D.; Barriga, J.; Celis, C.; Moreno, S.; Pérez, A. Degradation of crystal violet by catalytic wet peroxide oxidation (CWPO) with mixed Mn/Cu oxides. *Catalysts* **2019**, *9*, 530. [[CrossRef](#)]
36. Zielinski, J.; Zglinicka, I.; Znak, L.; Kaszukur, Z. Reduction of Fe₂O₃ with hydrogen. *App. Catal. A Gen.* **2010**, *381*, 191–196. [[CrossRef](#)]
37. Leofanti, G.; Padovan, M.; Tozzola, G.; Venturelli, B. Surface area and pore texture of catalysts. *Catal. Today* **1998**, *41*, 207–219. [[CrossRef](#)]
38. Gregg, S.J.; Sing, K.S.W. *Adsorption, Surface Area and Porosity*, 2nd ed.; Academic Press: London, UK, 1982.
39. Medeiros, R.; Macedo, H.P.; Melo, V.; Oliveira, A.; Barros, J.; Melo, M.; Melo, D. Ni supported on Fe-doped MgAl₂O₄ for dry reforming of methane: Use of factorial design to optimize H₂ yield. *Int. J. Hydrog. Energy* **2016**, *41*, 14047–14057. [[CrossRef](#)]
40. Özdemir, H.; Faruk, M.A.; Gürkaynak, M.A. Effect of the calcination temperature on Ni/MgAl₂O₄ catalyst structure and catalytic properties for partial oxidation of methane. *Fuel* **2014**, *116*, 63–70. [[CrossRef](#)]
41. Daza, C.E.; Gallego, J.; Moreno, J.A.; Mondragón, F.; Moreno, S.; Molina, R. CO₂ reforming of methane over Ni/Mg/Al/Ce mixed oxides. *Catal. Today* **2008**, *133–135*, 357–366. [[CrossRef](#)]
42. De Souza, G.; Ávila, V.C.; Marcílio, N.R.; Perez-Lopez, O.W. Synthesis Gas Production by Steam Reforming of Ethanol over M-Ni-Al Hydrotalcite-type Catalysts; M = Mg, Zn, Mo, Co. *Procedia Eng.* **2012**, *42*, 1805–1815. [[CrossRef](#)]

43. Choo, H.; Lam, S.; Sin, J.; Mohamed, A. An efficient Ag_2SO_4 -deposited ZnO in photocatalytic removal of indigo carmine and phenol under outdoor light irradiation. *Desalin. Water Treat.* **2015**, *57*, 14227–14240. [[CrossRef](#)]
44. Wang, W.; Zhu, Q.; Qin, F.; Dai, Q.; Wang, X. Fe doped CeO_2 nanosheets as Fentonlike heterogeneous catalysts for degradation of salicylic acid. *Chem. Eng. J.* **2018**, *333*, 226–239. [[CrossRef](#)]
45. Wanga, P.; Liang, Y.; Zhong, Z.; Hu, X. Nano-hybrid bimetallic Au-Pd catalysts for ambient condition-catalytic wet air oxidation (AC-CWAO) of organic dyes. *Sep. Purif. Technol.* **2020**, *233*, 115960. [[CrossRef](#)]



© 2020 by the authors. Licensee MDPI, Basel, Switzerland. This article is an open access article distributed under the terms and conditions of the Creative Commons Attribution (CC BY) license (<http://creativecommons.org/licenses/by/4.0/>).